Finding Regions of Counterfactual Explanations via Robust Optimization

Donato Maragno, Jannis Kurtz, Tabea E. Röber, Rob Goedhart, Ş. İlker Birbil, Dick den Hertog

Amsterdam Business School, University of Amsterdam, 1018TV Amsterdam, Netherlands

d.maragno@uva.nl j.kurtz@uva.nl t.e.rober@uva.nl r.goedhart2@uva.nl s.i.birbil@uva.nl d.denhertog@uva.nl

Counterfactual explanations play an important role in detecting bias and improving the explainability of data-driven classification models. A counterfactual explanation (CE) is a minimal perturbed data point for which the decision of the model changes. Most of the existing methods can only provide one CE, which may not be achievable for the user. In this work we derive an iterative method to calculate robust CEs, *i.e.* CEs that remain valid even after the features are slightly perturbed. To this end, our method provides a whole region of CEs allowing the user to choose a suitable recourse to obtain a desired outcome. We use algorithmic ideas from robust optimization and prove convergence results for the most common machine learning methods including decision trees, tree ensembles, and neural networks. Our experiments show that our method can efficiently generate globally optimal robust CEs for a variety of common data sets and classification models.

Key words: counterfactual explanation; explainable AI; machine learning; robust optimization

1. Introduction

Counterfactual explanations, also known as algorithmic recourse, are becoming increasingly popular as a way to explain the decisions made by black-box machine learning (ML) models. Given a factual instance for which we want to derive an explanation, we search for a counterfactual feature combination describing the minimum change in the feature space that will lead to a flipped model prediction. For example, for a person with a rejected loan application, the counterfactual explanation (CE) could be "if the *annual salary* would increase to 50,000\$, then the *loan application* would be approved." This method enables a form of user agency and is therefore particularly attractive in consequential decision making, where the user is directly and indirectly impacted by the outcome of the ML model.

The first optimization-based approach to generate CEs has been proposed by Wachter et al. (2018). Given a trained classifier $h : \mathcal{X} \to [0,1]$ and a *factual instance* $\hat{\boldsymbol{x}} \in \mathcal{X}$, the aim

is to find a *counterfactual* $\tilde{\boldsymbol{x}} \in \mathcal{X}$ that has the shortest distance to $\hat{\boldsymbol{x}}$, and has the opposite target. The problem to obtain $\tilde{\boldsymbol{x}}$ can be formulated as

$$\underset{\boldsymbol{x} \in \mathcal{X}}{\text{minimize}} \quad d(\hat{\boldsymbol{x}}, \boldsymbol{x}) \tag{1}$$

$$\text{subject to} \quad h(\boldsymbol{x}) \geq \tau, \tag{2}$$

where $d(\cdot, \cdot)$ is a distance function, often chosen to be the ℓ_1-norm or the ℓ_2-norm, and $\tau \in [0, 1]$ is a given threshold parameter for the classification decision.

Others have built on this work and proposed approaches that generate CEs with increased practical value, primarily by adding constraints to ensure actionability of the proposed changes and generating CEs that are close to the data manifold (Ustun et al. 2019, Russell 2019, Mahajan et al. 2019, Mothilal et al. 2020, Maragno et al. 2022). Nonetheless, the user agency provided by these methods remains theoretical: the generated CEs are exact point solutions that may remain difficult if not impossible to implement in practice. A minimal change to the proposed CE could fail to flip the model's prediction, especially since the CEs are close to the decision boundary due to minimizing the distance between $\hat{x}$ and $\tilde{x}$. As a solution, prior work suggests generating several CEs to increase the likelihood of generating at least one attainable solution. Approaches generating several CEs typically require solving the optimization problem multiple times (Russell 2019, Mothilal et al. 2020, Kanamori et al. 2021, Karimi et al. 2020), which might heavily affect the optimization time when the number of explanations is large. Maragno et al. (2022) suggest using incumbent solutions, however, this does not allow to control the quality of sub-optimal solutions. On top of that, the added practical value may be unconvincing: each of the CEs is still sensitive to arbitrarily small changes in the actions implemented by the user (Dominguez-Olmedo et al. 2021, Pawelczyk et al. 2022, Virgolin and Fracaros 2023).

This problem has been acknowledged in prior work and falls under the discussion of robustness in CEs. In the literature, the concept of robustness in CEs has different meanings: (1) robustness to input perturbations (Slack et al. 2021, Artelt et al. 2021), (2) robustness to model changes (Rawal et al. 2020, Forel et al. 2022, Upadhyay et al. 2021, Ferrario and Loi 2022, Black et al. 2021, Dutta et al. 2022, Bui et al. 2022), (3) robustness to hyperparameter selection (Dandl et al. 2020), and (4) robustness to recourse (Pawelczyk et al. 2022, Dominguez-Olmedo et al. 2021, Virgolin and Fracaros 2023). The latter

perspective, albeit very user-centered, has so far received only a little attention. Our work focuses on the latter definition of robustness in CEs, specifically, the idea of robustness to recourse. This means that a counterfactual solution should remain valid even if small changes are made to the implemented recourse action. In other words, we aim to define regions of counterfactual solutions that allow the user to choose any point within that region to flip the model prediction. While existing research has tackled this problem, their solutions are not comprehensive and have room for further improvements. In the remainder of this section, we will explore the related prior work and present our own contributions to this field.

Pawelczyk et al. (2022) introduce the notion of recourse invalidation rate, which amounts to the proportion of recourse that does not lead to the desired model prediction, *i.e.*, that is invalid. They model the noise around a counterfactual data point with a Gaussian distribution and suggest an approach that ensures the invalidation rate within a specified neighborhood around the counterfactual data point to be no larger than a target recourse invalidation rate. However, their work provides a heuristic solution using a gradient-based approach, which makes it not applicable to decision tree models. Additionally, it only provides a probabilistic robustness guarantee. Dominguez-Olmedo et al. (2021) introduce an approach where the optimal solution is surrounded by an uncertainty set such that every point in the set is a feasible solution. They also model causality between (perturbed) features to obtain a more informative neighborhood of similar points. Given a structural causal model (SCM), they model such perturbations as additive interventions on the factual instance features. The authors design an iterative approach that works only for differentiable classifiers and does not guarantee that the generated recourse actions are adversarially robust. Virgolin and Fracaros (2023) incorporate the possibility of additional intervention to contrast perturbations in their search for CEs. They make a distinction between the features that could be changed and those that should be kept as they are, and introduce the concept of C-setbacks; a subset of perturbations in changeable features that work against the user. Rather than seeking CEs that are not invalidated by C-setbacks, they seek CEs for which the additional intervention cost to overcome the setback is minimal. Perturbations to features that should be kept as they are according to a CE are orthogonal to the direction of the counterfactual, and Virgolin and Fracaros (2023) approximate a robustness-score for such features. A drawback of this method is that it is only

applicable in situations where additional intervention is possible, and not in situations where (*e.g.*, due to time limitations) only a single recourse is possible.

Our work addresses robustness to recourse by utilizing a robust optimization approach to generate regions of CEs. For a given factual instance, our method generates a set of CEs such that every solution in this set is a valid CE. This approach gives the user more flexibility in selecting a solution that best suits their needs. Additionally, the generated CEs are optimal in terms of their objective distance to the factual instance. The proposed algorithm is proven to converge, ensuring that the optimal solution is reached. This is different from prior work that provides only heuristic algorithms which are not provably able to find the optimal (i.e., closest) counterfactual point with a certain robustness guarantee (*e.g.,* Pawelczyk et al. 2022, Dominguez-Olmedo et al. 2021). Unlike prior research in this area, our approach is able to provide deterministic robustness guarantees for the CEs generated. Furthermore, our method does not require differentiability of the underlying ML model and is applicable to the tree-based models, which, to the best of our knowledge, has not been done before.

In summary, we make the following contributions:

• We propose an iterative algorithm that effectively finds global optimal robust CEs for trained decision trees, ensembles of trees, and neural networks.

• We prove the convergence of the algorithm for the considered trained models.

• We demonstrate the power of our algorithm on several datasets and different ML models. We empirically evaluate its convergence performance and compare the robustness as well as the validity of the generated CEs with the prior work in the literature.

• We release an open-source software called RCE to make the proposed algorithm easily accessible to practitioners. Our software is available in a dedicated repository[1] through which all our results can be reproduced.

2.   Robust Counterfactual Explanations

We consider binary classification problems, *i.e.*, we have a trained classifier $h : \mathcal{X} \to [0, 1]$ that assigns a value between zero and one to each data point in the data space $\mathcal{X} \subseteq \mathbb{R}^n$. A point $\boldsymbol{x} \in \mathcal{X}$ is then predicted to correspond to class $+1$, if $h(\boldsymbol{x}) \geq \tau$ and to class -1, otherwise. Here $\tau \in [0, 1]$ is a given threshold parameter which is often chosen to be $\tau = 0.5$.

---

[1]https://github.com/donato-maragno/robust-CE

Given a factual instance $\hat{\boldsymbol{x}} \in \mathcal{X}$ which is predicted to be in class -1, *i.e.*, $h(\hat{\boldsymbol{x}}) < \tau$, the robust CE problem is defined as

$$\underset{\boldsymbol{x} \in \mathcal{X}}{\text{minimize}} \quad d(\boldsymbol{x}, \hat{\boldsymbol{x}}) \tag{3}$$

$$\text{subject to} \quad h(\boldsymbol{x} + \boldsymbol{s}) \geq \tau, \quad \forall \boldsymbol{s} \in \mathcal{S}, \tag{4}$$

where the $d(\boldsymbol{x}, \hat{\boldsymbol{x}})$ represents a distance function, *e.g.*, induced by the ℓ_1-, ℓ_2- or ℓ_∞-norm, and $\mathcal{S} \subset \mathbb{R}^n$ is a given uncertainty set. The idea of the problem is to find a point that is as close as possible to the factual instance $\hat{\boldsymbol{x}}$ such that for all perturbations $\boldsymbol{s} \in \mathcal{S}$, the corresponding point $\boldsymbol{x} + \boldsymbol{s}$ is classified as $+1$ which is enforced by constraints (4); see Figure 1. This results in a large set of counterfactual explanations.

We consider uncertainty sets of the type

$$\mathcal{S} = \{\boldsymbol{s} \in \mathbb{R}^n \ | \ ||\boldsymbol{s}|| \leq \rho\}, \tag{5}$$

where $\| \cdot \|$ is a given norm. Popular choices are the ℓ_∞-norm, resulting in a box with upper and lower bounds on features, or the ℓ_2-norm, resulting in a circular uncertainty set. We refer to Ben-Tal et al. (2009) for a discussion of uncertainty sets. From the user perspective, choosing the ℓ_∞-norm has a practical advantage since the region $\mathcal{S}$ is a box, *i.e.*, we obtain an interval for each attribute of $\hat{\boldsymbol{x}}$. Each attribute can be changed in its corresponding interval independently, resulting in a counterfactual explanation. Hence, the user can easily detect if there exists a CE in the region which can be practically reached. We note that the model in (3)-(4) has infinitely many constraints. One approach often used in robust optimization is to rewrite constraints (4) as

$$\min_{\boldsymbol{s} \in \mathcal{S}} h(\boldsymbol{x} + \boldsymbol{s}) \geq \tau,$$

and dualize the optimization problem on the left hand side. This leads to a problem with a finite number of constraints. Unfortunately, strong duality is required to perform this reformulation, which does not hold for most classifiers h involving non-convexity or integer variables[2]. In the latter case, we can use an alternative method popular in robust optimization where the constraints are generated iteratively. This iterative approach to

---

[2]See Appendix A for the well-known dual approach applied to linear models.
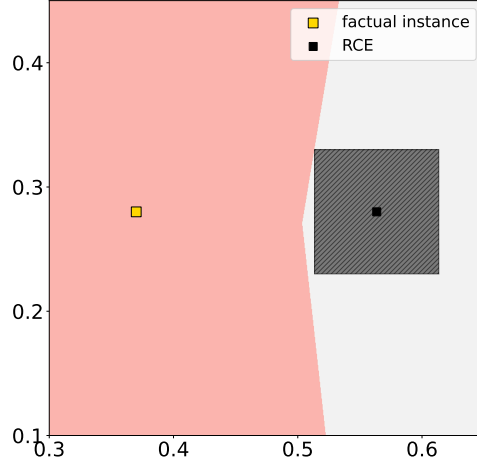
Figure 1   **Robust CE for a neural network and using a box uncertainty set. All points in the red region are classified as** -1**, all points in the white region as** $+1$**.**

solve problem (3)-(4) is known as the *adversarial approach*. The idea is to consider a relaxed version of the model, where only a finite subset of scenarios $\mathcal{Z} \subset \mathcal{S}$ is considered:

$$\underset{\boldsymbol{x} \in \mathcal{X}}{\text{minimize}} \quad d(\boldsymbol{x}, \hat{\boldsymbol{x}}) \tag{MP}$$

$$\text{subject to} \quad h(\boldsymbol{x} + \boldsymbol{s}) \geq \tau, \quad \forall \boldsymbol{s} \in \mathcal{Z}. \tag{6}$$

This problem is called the *master problem* (MP), and it only has a finite number of constraints. Note that the optimal value of (MP) is a lower bound of the optimal value of (3)-(4). However, an optimal solution $\boldsymbol{x}^*$ of (MP) is not necessarily feasible for the original problem, since there may exist a scenario in $\mathcal{S}$ that is not contained in $\mathcal{Z}$ for which the solution is not feasible. More precisely, it may be that there exists an $\boldsymbol{s} \in \mathcal{S}$ such that $h(\boldsymbol{x}^* + \boldsymbol{s}) < \tau$, and hence, $\boldsymbol{x}^*$ is not a robust counterfactual. In this case, we want to find such a scenario $\boldsymbol{s}^*$ that makes solution $\boldsymbol{x}^*$ infeasible. This can be done by solving the following, so called, *adversarial problem* (AP):

$$\underset{\boldsymbol{s} \in \mathcal{S}}{\max} \ \tau - h(\boldsymbol{x}^* + \boldsymbol{s}). \tag{AP}$$

The idea is to find a scenario $\boldsymbol{s}^* \in \mathcal{S}$ such that the prediction of classifier h for point $\boldsymbol{x}^* + \boldsymbol{s}^*$ is -1, *i.e.*, $\tau - h(\boldsymbol{x}^* + \boldsymbol{s}^*) > 0$. If we can find such a scenario and add it to the set $\mathcal{Z}$ in the MP, then $\boldsymbol{x}^*$ cannot be feasible anymore for (MP). To find the scenario with the largest impact, we maximize the constraint violation in the objective function in (AP). If the optimal value of (AP) is positive then $\boldsymbol{x}^* + \boldsymbol{s}^*$ is classified as -1, and the optimal solution
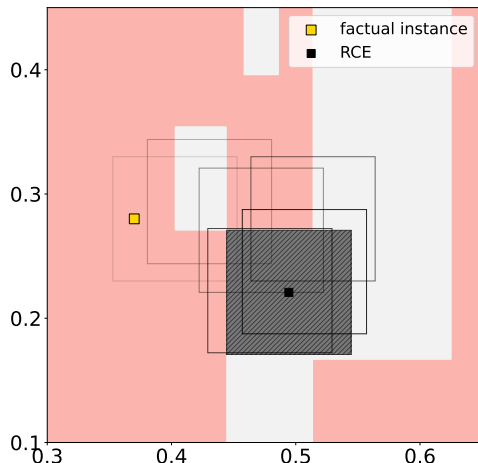
Figure 2 Iterations of Algorithm 1 to find the optimal robust CE for a decision tree. For each (MP) solution, we show the uncertainty box around it. As long as the box overlaps with the red region, a new scenario can be found and the solution moves in the next iteration.

Algorithm 1 Adversarial Algorithm

Input: $\mathcal{S}$, $\hat{\boldsymbol{x}}$, $\varepsilon > 0$

$\mathcal{Z} = \{\boldsymbol{0}\}$

repeat

$\quad \boldsymbol{x}^* \leftarrow$ Solve (MP) with $\mathcal{Z}, \hat{\boldsymbol{x}}$

$\quad \boldsymbol{s}^*, \mathrm{opt} \leftarrow$ Solve (AP) with $\boldsymbol{x}^*, \mathcal{S}$

$\quad \mathcal{Z} \leftarrow \mathcal{Z} \cup \{\boldsymbol{s}^*\}$

until $\mathrm{opt} \leq \varepsilon$

Return: x^*

$\boldsymbol{s}^*$ is added to $\mathcal{Z}$, and we calculate a solution $\boldsymbol{x}^*$ of the updated (MP). We iterate until no violating scenario can be found, that is, until the optimal value of (AP) is smaller or equal to zero. Note that in this case $h(\boldsymbol{x}^* + \boldsymbol{s}) \geq \tau$ holds for all $\boldsymbol{s} \in \mathcal{S}$, which means that $\boldsymbol{x}^*$ is a robust counterfactual. Algorithm 1 shows the steps of our approach, and Figure 2 shows its iterative behaviour. Each time a new scenario $\boldsymbol{s}$ is found by solving the AP, it is added to the uncertainty set $\mathcal{Z}$, and the new solution $\boldsymbol{x}^*$ moves to be feasible also for the new scenario. This is repeated until no scenario can be found anymore, *i.e.*, until the full box lies in the correct region. Note that instead of checking for a positive optimal value of (AP), we use an accuracy parameter $\varepsilon > 0$ in Algorithm 1. In this case, we can guarantee the convergence of our algorithm using the following result.

THEOREM 1 **(Mutapcic and Boyd, 2009)**. *If $\mathcal{X}$ is bounded and if h is a Lipschitz continuous function, i.e., there exists an $L > 0$ such that*

$$|h(\boldsymbol{x_1}) - h(\boldsymbol{x_2})| \leq L\|\boldsymbol{x_1} - \boldsymbol{x_2}\|$$

for all $\boldsymbol{x_1}, \boldsymbol{x_2} \in \mathcal{X}$. Then, for any tolerance parameter value $\epsilon > 0$, Algorithm 1 terminates after a finite number of steps with a solution $\boldsymbol{x}^*$ such that

$$h(\boldsymbol{x}^* + \boldsymbol{s}) \geq \tau - \varepsilon$$

for all $\boldsymbol{s} \in \mathcal{S}$.

Indeed without Lipschitz continuity, the convergence of Algorithm 1 cannot be ensured. We elaborate on this necessity in the following example, for which Algorithm 1 does not terminate in a finite number of steps.

EXAMPLE 1. Consider a classifier $h : \mathbb{R}^2 \to [0,1]$ with $h(\boldsymbol{x}) = 0$, if $x_2 > \frac{1}{2}$ and $h(\boldsymbol{x}) = 1$, otherwise. The threshold is $\tau = 0.5$, *i.e.*, a point is classified as 1, if $x_2 \leq \frac{1}{2}$ and as -1, otherwise. The factual instance is $\hat{\boldsymbol{z}} = (0,2)$, which is classified as -1. Furthermore, the uncertainty set is given as $\mathcal{S} = \{\boldsymbol{s} \in \mathbb{R}^2 : \|\boldsymbol{s}\|_\infty \leq 1\}$. We can warm-start Algorithm 1 with the (MP) solution $\boldsymbol{x}^1 = (0,0)$. Now, assume that in iteration i the optimal solution returned by (AP) is $\boldsymbol{s}^i = (1, \frac{1}{2} + \sum_{j=1}^{i} \left(\frac{1}{4}\right)^j)$. Note that in the first iteration $\boldsymbol{s}^1 = (1, \frac{3}{4})$ lies on the boundary of $\mathcal{S}$ and $\boldsymbol{x}^1 + \boldsymbol{s}^1$ is classified as -1, *i.e.*, it is an optimal solution of (AP). We are looking now for the closest point $\boldsymbol{x}^2$ to $\hat{\boldsymbol{x}}$ such that $\boldsymbol{x}^2 + \boldsymbol{s}^1$ is classified as 1, that is, it has a second component of at most $\frac{1}{2}$. This is the point $\boldsymbol{x}^2 = (0, -\frac{1}{4})$ which must be the optimal solution of (MP). Note that $\boldsymbol{s}^2$ is again on the boundary of $\mathcal{S}$ and $\boldsymbol{x}^2 + \boldsymbol{s}^2 = (1, \frac{1}{2} + \frac{1}{8})$ is classified as -1. Hence, $\boldsymbol{s}^2$ is an optimal solution of (AP). We can conclude inductively that the optimal solution of (MP) in iteration i is $\boldsymbol{x}^i = (0, -\sum_{j=1}^{i} \left(\frac{1}{4}\right)^j)$ and that $\boldsymbol{s}^i$ is an optimal solution of (AP) in iteration i. Note that the latter is true, since the value of h is constant in the negative region, and hence, each point in the uncertainty set is an optimal solution of (AP). If the latter solutions are returned by (AP), then the sequence of solutions $\boldsymbol{x}^i$ converges to the point $\bar{\boldsymbol{x}} = (0, -\frac{1}{3})$ which follows from the limit of the geometric series. However, $\bar{\boldsymbol{x}}$ is not a robust CE regarding S, since for instance, $\bar{\boldsymbol{x}} + (0,1) = (0, \frac{2}{3})$ is classified as -1. Consequently, Algorithm 1 never terminates. This example is illustrated in Figure 3.
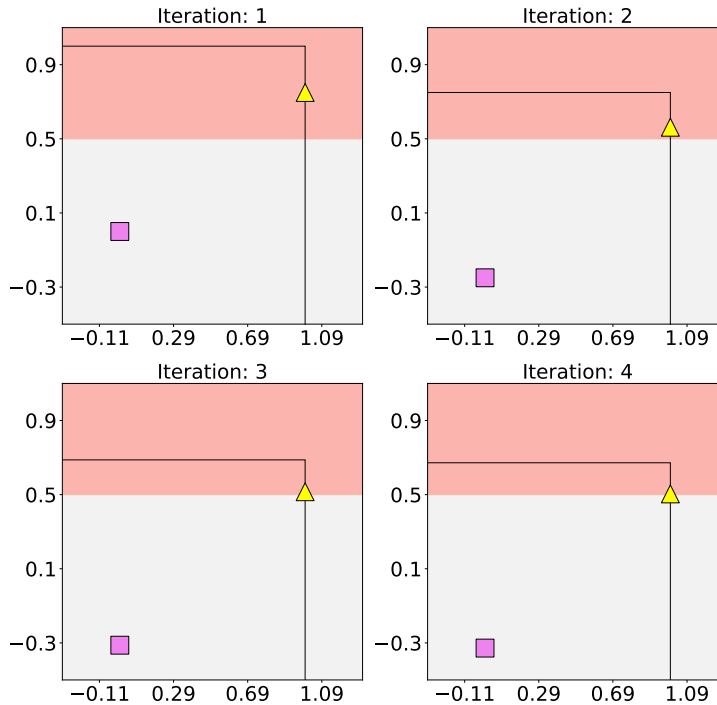
Figure 3 Illustration of the iterations of Algorithm 1 for the problem in Example 1. The purple square represents the current (MP) solution, while the yellow triangle represents the solution of the adversarial problem. The distance of the adversarial solutions to the decision boundary is $\left(\frac{1}{4}\right)^i$ in iteration i.

One difficulty is modeling the constraints of the form $h(\boldsymbol{x} + \boldsymbol{s}) \geq \tau$ for different trained classifiers. For decision trees, ensembles of decision trees, and neural networks, these constraints can be modeled by mixed-integer linear constraints as we present in the following section. Another difficulty is that h is discontinuous for decision trees and ensembles of decision trees. To handle these models, we have to find Lipschitz continuous extensions of h with equivalent predictions to guarantee convergence of Algorithm 1.

3. Trained Models

In this section, we give reformulations for (MP) and (AP) –specifically for decision trees, tree ensembles, and neural networks– that satisfy the conditions needed in Theorem 1 for convergence.

3.1. Decision Trees

A decision tree (DT) partitions the data samples into distinct *leaves* through a series of *feature splits*. A split at node j is performed by a hyperplane $\tilde{\boldsymbol{a}}_j^\top \boldsymbol{x} = \tilde{b}_j$. We assume that $\tilde{\boldsymbol{a}_j}$ can have multiple non-zero elements, in which we have the hyperplane split setting – if there is only one non-zero element, this creates an orthogonal (single feature) split. We

denote the index-set of all split nodes j by $\mathcal{N}$. Then, each leaf i of the tree is given by a subset of splits $\mathcal{N}^i_{\leq} \subseteq \mathcal{N}$ and $\mathcal{N}^i_{<} \subseteq \mathcal{N}$, where $N^i_{\leq} \cap N^i_{<} = \emptyset$. Formally, we define

$$\mathcal{L}_i = \{\boldsymbol{x} \in X : \boldsymbol{a}_{\boldsymbol{j}}^\top \boldsymbol{x} \leq b_j, j \in \mathcal{N}^i_{\leq};\ \boldsymbol{a}_{\boldsymbol{j}}^\top \boldsymbol{x} < b_j, j \in \mathcal{N}^i_{<} \}.$$

Furthermore, it always holds that $\mathbb{R}^n = \bigcup_{i \in \mathcal{L}} \mathcal{L}_i$, where $\mathcal{L}$ is the index set of all leaves, and $\mathcal{L}_i \cap \mathcal{L}_k = \emptyset$ for every pair $i \neq k$. Each leaf i is assigned a weight $p_i \in [0, 1]$, which is normally determined by the fraction of training data of class 1 inside the leaf. The classifier is a piecewise constant function h, where $h(\boldsymbol{x}) = p_i$ if and only if $\boldsymbol{x}$ is contained in leaf i. Since, h is a discontinuous step-function, and it is not Lipschitz continuous. To achieve convergence of our algorithm, we have to find a Lipschitz continuous function assigning the same classes to each data point as h. To this end we define the function

$$\tilde{h}(\boldsymbol{x}) = \begin{cases} \tau, & \boldsymbol{x} \in \mathcal{L}_i, p_i \geq \tau; \\ \tau - \min_{j \in \mathcal{N}^i_{\leq} \cup \mathcal{N}^i_{<}} b_j - \boldsymbol{a}_{\boldsymbol{j}}^\top \boldsymbol{x}, & \boldsymbol{x} \in \mathcal{L}_i, p_i < \tau. \end{cases}$$

We choose this function to have a constant value of τ for all leaves with $p_i \geq \tau$ while for a point $\boldsymbol{x}$ in one of the other leaves, we subtract from τ the minimum slack-value of the point over all leaf-defining constraints. Since the minimum slack on the boundary of the leaves is zero, $\tilde{h}$ is a continuous function and it holds $\tilde{h}(\boldsymbol{x}) < \tau$ in the interior of the latter leaves. Note that the value of h decreases if we a point is more far away from the boundary of the leaf. Unfortunately, due to imposed continuity, the predictions on the boundaries of the leaves can be different than the original predictions of h. We show in the following lemma that $\tilde{h}$ is Lipschitz continuous and, except on the leaf boundaries, the same class is assigned to each data point as it is done by the original classifier h.

LEMMA 1. *The function $\tilde{h}$ is Lipschitz continuous on $\mathcal{X}$ and $int\left(\{\boldsymbol{x} : \tilde{h}(\boldsymbol{x}) \geq \tau\}\right) \subseteq \{\boldsymbol{x} : h(\boldsymbol{x}) \geq \tau\} \subseteq \{\boldsymbol{x} : \tilde{h}(\boldsymbol{x}) \geq \tau\}$, where $int(\cdot)$ denotes the interior of the set.*

Proof. We first show, that $\tilde{h}$ is Lipschitz continuous. To this end, let $\boldsymbol{x}, \boldsymbol{y} \in \mathcal{X}$. Consider the following three cases. *Case 1:* Both points are contained in a leaf with prediction 1, i.e., $\boldsymbol{x} \in \mathcal{L}_i$ and $\boldsymbol{y} \in \mathcal{L}_{i'}$ with $p_i, p_{i'} \geq \tau$. In this case we have

$$|\tilde{h}(\boldsymbol{x}) - \tilde{h}(\boldsymbol{y})| = |\tau - \tau| = 0 \leq \|\boldsymbol{x} - \boldsymbol{y}\|. \tag{7}$$

Case 2: Point $\boldsymbol{x}$ is in a leaf with prediction 1, and point $\boldsymbol{y}$ is in a leaf with prediction -1, i.e., $\boldsymbol{x} \in \mathcal{L}_i$ and $\boldsymbol{y} \in \mathcal{L}_{i'}$ with $p_i \geq \tau$ and $p_{i'} < \tau$. Since $\boldsymbol{x}$ is not contained in $\mathcal{L}_{i'}$, there must be one node j^* (without loss of generality, we assume that $j^* \in \mathcal{N}_{\leq}^{i'}$) such that $\boldsymbol{a}_{j^*}^\top \boldsymbol{y} \leq b_{j^*}$ and $\boldsymbol{a}_{j^*}^\top \boldsymbol{x} > b_{j^*}$. It holds $\tilde{h}(\boldsymbol{x}) = \tau \geq \tilde{h}(\boldsymbol{y})$, and we obtain

$$|\tilde{h}(\boldsymbol{x}) - \tilde{h}(\boldsymbol{y})| = \tau - (\tau - \min_{j \in \mathcal{N}_{\leq}^{i'} \cup \mathcal{N}_{<}^{i'}} b_j - \boldsymbol{a}_j^\top \boldsymbol{y}) \tag{8}$$

$$= \min_{j \in \mathcal{N}_{\leq}^{i'} \cup \mathcal{N}_{<}^{i'}} b_j - \boldsymbol{a}_j^\top \boldsymbol{y} \tag{9}$$

$$\leq b_{j^*} - \boldsymbol{a}_{j^*}^\top \boldsymbol{y} \tag{10}$$

$$< b_{j^*} - \boldsymbol{a}_{j^*}^\top \boldsymbol{y} + \boldsymbol{a}_{j^*}^\top \boldsymbol{x} - b_{j^*} \tag{11}$$

$$= \boldsymbol{a}_{j^*}^\top (\boldsymbol{x} - \boldsymbol{y}) \tag{12}$$

$$\leq \|\boldsymbol{a}_{j^*}\| \|\boldsymbol{x} - \boldsymbol{y}\|, \tag{13}$$

where the first inequality follows from $j^* \in \mathcal{N}_{\leq}^{i'} \cup \mathcal{N}_{<}^{i'}$, the second inequality follows from $\boldsymbol{a}_{j^*}^\top \boldsymbol{x} > b_{j^*}$, and for the last inequality we apply the Cauchy-Schwarz inequality.

Case 3: Both points are contained in a leaf with prediction -1, i.e., $\boldsymbol{x} \in \mathcal{L}_i$ and $\boldsymbol{y} \in \mathcal{L}_{i'}$ with $p_i, p_{i'} < \tau$. First assume that $i \neq i'$. Without loss of generality, we also assume that $\tilde{h}(\boldsymbol{x}) \geq \tilde{h}(\boldsymbol{y})$. In this case, we have

$$|\tilde{h}(\boldsymbol{x}) - \tilde{h}(\boldsymbol{y})| \leq \tau - (\tau - \min_{j \in \mathcal{N}_{\leq}^{i'} \cup \mathcal{N}_{<}^{i'}} b_j - \boldsymbol{a}_j^\top \boldsymbol{y}), \tag{14}$$

which follows from $\tilde{h}(\boldsymbol{x}) \leq \tau$ for all $\boldsymbol{x} \in \mathcal{X}$. We can prove Lipschitz continuity in this case by following the same steps as in Case 2. When $i = i'$, we designate j^* as the index which attains the minimum in

$$\tau - \min_{j \in \mathcal{N}_{\leq}^i \cup \mathcal{N}_{<}^i} b_j - \boldsymbol{a}_j^\top \boldsymbol{x}. \tag{15}$$

Then, we have

$$|\tilde{h}(\boldsymbol{x}) - \tilde{h}(\boldsymbol{y})| = \tau - b_{j^*} + \boldsymbol{a}_{j^*}^\top \boldsymbol{x} - (\tau - \min_{j \in \mathcal{N}_{\leq}^{i'} \cup \mathcal{N}_{<}^{i'}} b_j - \boldsymbol{a}_j^\top \boldsymbol{y}) \tag{16}$$

$$\leq -b_{j^*} + \boldsymbol{a}_{j^*}^\top \boldsymbol{x} + b_{j^*} - \boldsymbol{a}_{j^*}^\top \boldsymbol{y} \tag{17}$$

$$= \boldsymbol{a}_{j^*}^\top (\boldsymbol{x} - \boldsymbol{y}) \tag{18}$$

$$\leq \|\boldsymbol{a}_{j^*}\| \|\boldsymbol{x} - \boldsymbol{y}\|, \tag{19}$$

where we use $j^* \in \mathcal{N}_{\leq}^{i'} \cup \mathcal{N}_{<}^{i'}$ for the first inequality, and the Cauchy-Schwarz inequality for the last one.

Following the three cases above, we show that $\tilde{h}$ is Lipschitz continuous with Lipschitz constant $L = \max_{j \in \mathcal{N}} \|\boldsymbol{a_j}\|$.

We now show the second part of the result. First, assume for $\boldsymbol{x}$ that $h(\boldsymbol{x}) \geq \tau$. This implies that $\boldsymbol{x}$ is contained in a leaf $\mathcal{L}_i$ with $p_i \geq \tau$, and hence, $\tilde{h}(\boldsymbol{x}) = \tau$ showing the second inclusion. For the first inclusion, let now $\boldsymbol{x}$ be a point in the interior of the set $\{\boldsymbol{x} : \tilde{h}(\boldsymbol{x}) \geq \tau\}$. Assume the contrary of the statement, *i.e.*, it is contained in a leaf $\mathcal{L}_i$ with $p_i < \tau$. We can assume that the leaf is full-dimensional, since otherwise the interior is empty. Then, by definition of $\tilde{h}$, it must hold that

$$\tau - \min_{j \in \mathcal{N}_{\leq}^i \cup \mathcal{N}_{<}^i} b_j - \boldsymbol{a_j}^\top \boldsymbol{x} \geq \tau. \tag{20}$$

That is, there is a node $j \in \mathcal{N}_{\leq}^i \cup \mathcal{N}_{<}^i$ such that $\boldsymbol{a_j}^\top \boldsymbol{x} = b_j$. Since the leaf is a full-dimensional polyhedron, there exists a $\bar{\delta} > 0$ and a direction $\boldsymbol{v}$ such that $\boldsymbol{a_j}^\top (\boldsymbol{x} + \delta \boldsymbol{v}) < b_j$ for all $0 < \delta < \bar{\delta}$ and all $j \in \mathcal{N}_{\leq}^i \cup \mathcal{N}_{<}^i$. Consequently, $\tilde{h}(\boldsymbol{x} + \delta \boldsymbol{v}) < \tau$ for all $0 < \delta < \bar{\delta}$. This implies that $\boldsymbol{x}$ cannot be in the interior of the set $\{\boldsymbol{x} : \tilde{h}(\boldsymbol{x}) \geq \tau\}$, which is a contradiction. Thus, $\boldsymbol{x}$ must be contained in a leaf with $p_i \geq \tau$ which proves the result. $\qquad\square$

We can now derive the formulations for (MP) and (AP) for our tree model. By using Lemma 1, we can use h instead of $\tilde{h}$ to model Constraints (6) in (MP). Then, we can adapt the decision tree formulation proposed by Maragno et al. (2022) and reformulate Constraint (6) of (MP) as

$$\boldsymbol{a_j}^\top (\boldsymbol{x} + \boldsymbol{s}) - M(1 - l_i(\boldsymbol{s})) \leq b_j, \ i \in \mathcal{L}, j \in \mathcal{N}_{\leq}^i, \boldsymbol{s} \in \mathcal{Z}, \tag{21}$$

$$\boldsymbol{a_j}^\top (\boldsymbol{x} + \boldsymbol{s}) - M(1 - l_i(\boldsymbol{s})) < b_j, \ i \in \mathcal{L}, j \in \mathcal{N}_{<}^i, \boldsymbol{s} \in \mathcal{Z}, \tag{22}$$

$$\sum_{i \in \mathcal{L}} l_i(\boldsymbol{s}) = 1, \quad \boldsymbol{s} \in \mathcal{Z}, \tag{23}$$

$$\sum_{i \in \mathcal{L}} l_i(\boldsymbol{s}) p_i \geq \tau, \quad \boldsymbol{s} \in \mathcal{Z}, \tag{24}$$

$$l_i(\boldsymbol{s}) \in \{0, 1\}, \quad i \in \mathcal{L}, \boldsymbol{s} \in \mathcal{Z}, \tag{25}$$

where M is a predefined large-enough constant. The variables $l_i(\boldsymbol{s})$ are binary variables associated with the corresponding leaf i and scenario $\boldsymbol{s}$, where $l_i(\boldsymbol{s}) = 1$, if solution $\boldsymbol{x} + \boldsymbol{s}$

is contained in leaf i. Constraints (23) ensure that each scenario gets assigned to exactly one leaf. Constraints (21) and (22) ensure that only if leaf i is selected for scenario $\boldsymbol{s}$, *i.e.*, $l_i(\boldsymbol{s}) = 1$, then $\boldsymbol{x} + \boldsymbol{s}$ has to fulfill the corresponding constraints of $\mathcal{L}_i$ while the constraints for all other leaves can be violated, which is ensured by the big-M value. Note that in our computational experiments we use an $\tilde{\varepsilon}$-accuracy parameter to reformulate the strict inequalities as non-strict inequalities. Finally, Constraints (24) ensure that the chosen leaf has a weight p_i which is greater than or equal to the threshold τ. We can remove all variables and constraints of the problem related to leaves with $p_i < \tau$ together with constraint (24), since only leafs which correspond to label $+1$ can be chosen to obtain a feasible solution.

Using the Lipschitz continuous function $\tilde{h}$, (AP) can be reformulated as

$$\tau + \max_{\boldsymbol{s} \in \mathcal{S}} -\tilde{h}(\boldsymbol{x}^* + \boldsymbol{s}). \tag{26}$$

Optimizing $-\tilde{h}(\boldsymbol{x}^* + \boldsymbol{s})$ over $\mathcal{S}$ is equivalent to iterating over all leaves $\mathcal{L}_i$ with $p_i < \tau$ and maximizing the same function over the corresponding leaf. The problem is formulated as:

$$\text{maximize} \quad -\tau + \min_{j \in \mathcal{N}^i_{\leq} \cup \mathcal{N}^i_{<}} \{b_j - \boldsymbol{a}_{\boldsymbol{j}}^\top (\boldsymbol{x}^* + \boldsymbol{s})\} \tag{27}$$

$$\text{subject to} \quad \boldsymbol{a}_{\boldsymbol{j}}^\top (\boldsymbol{x}^* + \boldsymbol{s}) \leq b_j, \quad j \in \mathcal{N}^i_{\leq}, \tag{28}$$

$$\boldsymbol{a}_{\boldsymbol{j}}^\top (\boldsymbol{x}^* + \boldsymbol{s}) < b_j, \quad j \in \mathcal{N}^i_{<}, \tag{29}$$

$$\boldsymbol{s} \in \mathcal{S} \tag{30}$$

for each such leaf. Using a level-set transformation and substituting the latter problem in (26) leads to

$$\text{maximize} \quad \alpha \tag{31}$$

$$\text{subject to} \quad \alpha \leq w_j, \quad j \in \mathcal{N}^i_{\leq} \cup \mathcal{N}^i_{<}, \tag{32}$$

$$\boldsymbol{a}_{\boldsymbol{j}}^\top (\boldsymbol{x}^* + \boldsymbol{s}) + w_j \leq b_j, \quad j \in \mathcal{N}^i_{\leq}, \tag{33}$$

$$\boldsymbol{a}_{\boldsymbol{j}}^\top (\boldsymbol{x}^* + \boldsymbol{s}) + w_j < b_j, \quad j \in \mathcal{N}^i_{<}, \tag{34}$$

$$\boldsymbol{s} \in \mathcal{S}, \boldsymbol{w} \geq 0, \tag{35}$$

which is equivalent to maximizing the minimum slacks of the constraints corresponding to the leaves. Geometrically this means that we try to find a perturbation $\boldsymbol{s}$ such that $\boldsymbol{x}^* + \boldsymbol{s}$ is as deep as possible in one of the negative leaves; see Figure 4. Note that the problems
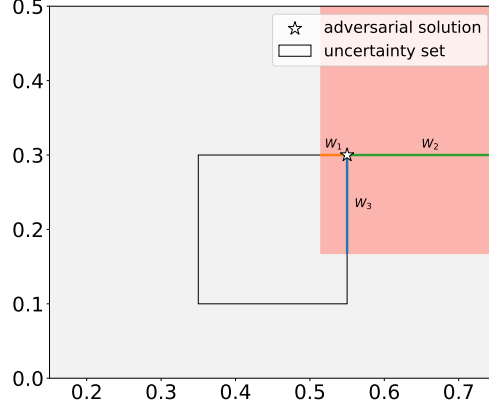
Figure 4   **Slack values of a solution regarding the leaf-defining constraints where the minimum slack is maximized.**

(31) are continuous optimization problems that can be solved efficiently by state-of-the-art solvers, such as, Gurobi Gurobi Optimization, LLC (2022) or CPLEX Cplex (2009).

Heuristic Variant. Using Algorithm 1 can be computationally demanding, since it requires solving (MP) and (AP) many times in an iterative manner. An alternative and more efficient approach can be conducted, where we try to find a CE $\boldsymbol{x}^*$ that is robust only regarding to one leaf of the tree. More precisely, this means that $\boldsymbol{x}^* + \boldsymbol{s}$ is contained in the same leaf for all $\boldsymbol{s} \in \mathcal{S}$. This is an approximation, since for each scenario $\boldsymbol{s}$, the point $\boldsymbol{x}^* + \boldsymbol{s}$ could be contained in a different neighboring leaf leading to better CEs; see Figure 5. Hence, the solutions of the latter approach may be non-optimal. When restricting to one leaf, we can iterate over all possible leaves $\mathcal{L}_i$ with $p_i < \tau$ and solve the resulting (MP):

$$\text{minimize} \quad d(\boldsymbol{x}, \hat{\boldsymbol{x}}) \tag{36}$$

$$\text{subject to} \quad \boldsymbol{a}_j^\top \boldsymbol{x} + \rho ||\boldsymbol{a}_j||^* \leq b_j, \quad j \in \mathcal{N}_{\leq}^i, \tag{37}$$

$$\boldsymbol{a}_j^\top \boldsymbol{x} + \rho ||\boldsymbol{a}_j||^* < b_j, \quad j \in \mathcal{N}_{<}^i, \tag{38}$$

$$\boldsymbol{x} \in \mathcal{X}, \tag{39}$$

and choose the solution $\boldsymbol{x}^*$ for the leaf which yields the best optimal value. Note that, in that case, we do not need binary assignment variables anymore, since we only consider one leaf for (MP). Alternatively, we can obtain the same result modelling the entire decision tree using auxiliary binary variables, one for each leaf i with $p_i \geq \tau$.

3.2. Tree Ensembles

In the case of tree ensembles like random forest (RF) and gradient boosting machines (GBM), we model the validity constraints by formulating each base learner separately.
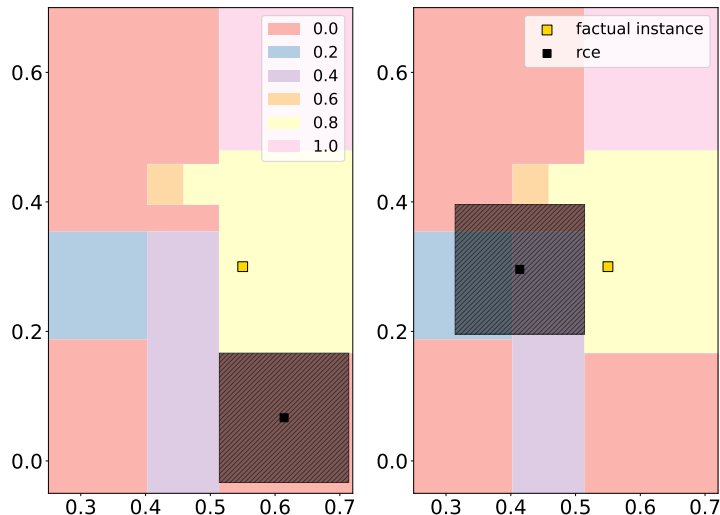
Figure 5   **(Left) the CE of the heuristic approach where the whole set is restricted to be contained in one leaf. (Right) an optimal CE where the uncertainty set can overlap over different leaves of a decision tree.**

Assume we obtain K base learners. Since each base learner is a decision tree, we can use the construction of the constraints (21)-(25) and apply them to all base learners separately. Then, we add the constraints to the master problem, where each base learner k gets a separate copy $l_i(\boldsymbol{s})(k)$ of the assignment variables and has its own set of node inequalities given by $\boldsymbol{a_j(k)}$ and $b_j(k)$. Additionally, we have to replace constraint (24) by

$$\frac{\sum_{k=1}^{K}\sum_{i\in\mathcal{L}}l_i(\boldsymbol{s})(k)p_i(k)}{K}\geq\tau, \tag{40}$$

where $p_i(k)$ is the weight of leaf i in base learner k. This constraint forces the average prediction value of the tree ensemble to be larger than or equal to τ. Note that to model a majority vote, we can use $p_i(k)\in\{0,1\}$. Since a random forest is equivalent to a decision tree, the same methodology for (AP) can be used as in Section 3.1. Note that for classical DTs we may iterate over all leaves and solve Problem (31). However, deriving the polyhedral descriptions of all leaves for an ensemble of trees is very time consuming. Instead (AP) can be reformulated as

$$\text{maximize} \quad \alpha \tag{41}$$

$$\text{subject to} \quad \alpha\leq w_j^k, \quad j\in\mathcal{N}_{\leq}^i(k)\cup\mathcal{N}_{<}^i(k),\ \forall k\in[K], \tag{42}$$

$$\boldsymbol{a_j(k)}^{\top}(\boldsymbol{x}^*+\boldsymbol{s})+w_j^k\leq b_j(k), \quad j\in\mathcal{N}_{\leq}^i(k),\ \forall k\in[K], \tag{43}$$

$$\boldsymbol{a_j(k)}^{\top}(\boldsymbol{x}^*+\boldsymbol{s})+w_j^k< b_j(k), \quad j\in\mathcal{N}_{<}^i(k),\ \forall k\in[K], \tag{44}$$

$$\boldsymbol{s}\in\mathcal{S},\ \ \boldsymbol{w}^k\geq0, \quad \forall k\in[K], \tag{45}$$

where $\mathcal{N}_{\leq}^i(k), \mathcal{N}_{<}^i(k)$ are the indices of the nodes of tree k as defined in Section 3.1 and we use $[K]$ to denote the set of the first K positive integers, that is $[K] = \{1, \ldots, K\}$.

Finally, note that since the classifier of an ensemble of trees is equivalent to a classical decision tree classifier, the convergence analysis presented in Section 3.1 holds also for the ensemble case.

3.3. Neural Networks

In the case of neural networks convergence of Algorithm 1 is immediately guaranteed when we consider ReLU activation functions. More precisely, the evaluation function $h : \mathcal{X} \to [0, 1]$ of a trained neural network with rectified linear unit (ReLU) activation functions is Lipschitz continuous, since it is a concatenation of Lipschitz continuous functions; see Appendix B for a formal proof.

Moreover, neural networks with ReLU activation functions belong to the MIP-representable class of ML models (Grimstad and Andersson 2019, Anderson et al. 2020). The ReLU operator of a neuron in layer l is given by

$$v_i^l = \max \left\{ 0, \beta_{i0}^l + \sum_{j \in N^{l-1}} \beta_{ij}^l v_j^{l-1} \right\}, \tag{46}$$

where $\boldsymbol{\beta}_i^l$ is the coefficient vector for neuron i in layer l, β_{i0}^l is the bias value and v_j^{l-1} is the output of neuron j of layer $l - 1$. Note that in our model the input of the neural network can be a data point $\boldsymbol{x}$ perturbed by a scenario $\boldsymbol{s}$, *i.e.*, all variables depend on the perturbation $\boldsymbol{s}$. The input in the first layer is $\boldsymbol{v}^0(\boldsymbol{s}) = \boldsymbol{x} + \boldsymbol{s}$ and the output of layer l is denoted as $v_j^l(\boldsymbol{s})$. The ReLU operator (46) can then be linearly reformulated as

$$v_i^l(\boldsymbol{s}) \geq \beta_{i0}^l + \sum_{j \in \mathcal{N}^{l-1}} \beta_{ij}^l v_j^{l-1,s}, \quad \boldsymbol{s} \in \mathcal{Z}, \tag{47}$$

$$v_i^l(\boldsymbol{s}) \leq \beta_{i0}^l + \sum_{j \in \mathcal{N}^{l-1}} \beta_{ij}^l v_j^{l-1,s} + M_{LB}(1 - l_i^l(\boldsymbol{s})), \quad \boldsymbol{s} \in \mathcal{Z}, \tag{48}$$

$$v_i^l(\boldsymbol{s}) \leq M_{UB} l_i^l(\boldsymbol{s}), \ \boldsymbol{s} \in \mathcal{Z}, \tag{49}$$

$$v_i^l(\boldsymbol{s}) \geq 0, \quad \boldsymbol{s} \in \mathcal{Z}, \tag{50}$$

$$l_i^l(\boldsymbol{s}) \in \{0, 1\}, \quad \boldsymbol{s} \in \mathcal{Z}, \tag{51}$$

where M_{LB} and M_{UB} are big-M values.

The following is a complete formulation of the master problem (MP) in the case of neural networks with ReLU activation functions:

$$\underset{\boldsymbol{x}\in\mathcal{X}}{\text{minimize}} \quad d(\boldsymbol{x},\hat{\boldsymbol{x}}) \tag{52}$$

$$\text{subject to} \quad \sum_{j\in\mathcal{N}^L}\beta_j^L v_j^{L-1}(\boldsymbol{s}) \geq \tau, \quad \boldsymbol{s}\in\mathcal{Z}, \tag{53}$$

$$v_i^l(\boldsymbol{s}) \geq \beta_{i0}^l + \sum_{j\in\mathcal{N}^{l-1}}\beta_{ij}^l v_j^{l-1}(\boldsymbol{s}), \quad \boldsymbol{s}\in\mathcal{Z}, \ i\in\mathcal{N}^l, \ \forall l\in[L], \tag{54}$$

$$v_i^l(\boldsymbol{s}) \leq \beta_{i0}^l + \sum_{j\in\mathcal{N}^{l-1}}\beta_{ij}^l v_j^{l-1}(\boldsymbol{s}) + M_{LB}(1-l_i^l(\boldsymbol{s})), \quad \boldsymbol{s}\in\mathcal{Z}, \ i\in\mathcal{N}^l, \ \forall l\in[L], \tag{55}$$

$$v_i^l(\boldsymbol{s}) \leq M_{UB}l_i^l(\boldsymbol{s}), \ \boldsymbol{s}\in\mathcal{Z}, \ i\in\mathcal{N}^l, \ \forall l\in[L], \tag{56}$$

$$v_i^0(\boldsymbol{s}) = x_i + s_i, \quad \boldsymbol{s}\in\mathcal{Z}, \ \forall i\in[n], \tag{57}$$

$$v_i^l(\boldsymbol{s}) \geq 0, \quad \boldsymbol{s}\in\mathcal{Z}, \ i\in\mathcal{N}^l, \ \forall l\in[L], \tag{58}$$

$$l_i^l(\boldsymbol{s}) \in \{0,1\}, \quad \boldsymbol{s}\in\mathcal{Z}, \ i\in\mathcal{N}^l, \ \forall l\in[L], \tag{59}$$

where L represents the number of layers with $[L]=\{1,\ldots,L\}$ and $\mathcal{N}^l$ the set of neurons in layer l. The first $L-1$ layers are activated by a ReLU function except for the output layer, which consists of a single node that is a linear combination of the node values in layer $L-1$. The variable $v_i^l(\boldsymbol{s})$ is the output of the activation function in node i, layer l, and scenario $\boldsymbol{s}$.

Likewise, the adversarial problem (AP) is formulated as

$$\underset{\boldsymbol{s}\in\mathcal{S}}{\text{maximize}} \quad \tau - \sum_{j\in\mathcal{N}^L}\beta_j^L v_j^{L-1}, \tag{60}$$

$$\text{subject to} \quad v_i^l \geq \beta_{i0}^l + \sum_{j\in\mathcal{N}^{l-1}}\beta_{ij}^l v_j^{l-1}, \quad i\in\mathcal{N}^l, \ \forall l\in[L], \tag{61}$$

$$v_i^l \leq \beta_{i0}^l + \sum_{j\in\mathcal{N}^{l-1}}\beta_{ij}^l v_j^{l-1} + M_{LB}(1-l_i^l), \quad i\in\mathcal{N}^l, \ \forall l\in[L], \tag{62}$$

$$v_i^l \leq M_{UB}l_i^l, \ i\in\mathcal{N}^l, \ \forall l\in[L], \tag{63}$$

$$v_i^0 = s_i + x_i^*, \quad i=1,\ldots,n, \tag{64}$$

$$v_i^l \geq 0, \quad i\in\mathcal{N}^l, \ \forall l\in[L], \tag{65}$$

$$l_i^l \in \{0,1\}, \quad i\in\mathcal{N}^l, \ \forall l\in[L], \tag{66}$$

$$\boldsymbol{s}\in\mathcal{S}, \tag{67}$$

where $\boldsymbol{x}^*$ is the counterfactual solution of (MP).

4. Experiments

In this section, we aim to illustrate the effectiveness of our method by conducting empirical experiments on various datasets. The mixed-integer optimization formulations of the ML models used in our experiments are based on Maragno et al. (2021). The experiments are being run on a computer with an Apple M1 Pro processor and 16 GB of RAM. For reproducibility, our open-source implementation can be found at our repository[3]. It is important to note that to the best of our knowledge, the present work is the first approach that generates a region of CEs for a range of different models, involving non-differentiable models. Therefore, a comparison to prior work is only possible with Dominguez-Olmedo et al. (2021) for the case of neural networks with ReLU activation functions.

		BANKNOTE AUTHENTICATION 4 features			DIABETES 8 features			IONOSPHERE 34 features		
Model	Specs	Comp. time (s)	# iterations	# early stops	Comp. time (s)	# iterations	# early stops	Comp. time (s)	# iterations	# early stops
					$\rho = 0.01$					
Linear	ElasticNet	0.25 (0.01)	–	–	0.23 (0.01)	–	–	0.25 (0.01)	–	–
DT	max depth: 3	1.53 (0.04)	1.00 (0.00)	–	1.66 (0.07)	1.20 (0.09)	–	1.66 (0.07)	1.10 (0.07)	–
	max depth: 5	1.86 (0.09)	1.10 (0.07)	–	2.29 (0.11)	1.20 (0.09)	–	1.96 (0.08)	1.10 (0.07)	–
	max depth: 10	3.90 (0.88)	2.00 (0.58)	–	5.77 (0.48)	1.40 (0.13)	–	2.86 (0.16)	1.20 (0.09)	–
RF*	# est.: 5	3.50 (0.36)	1.75 (0.22)	–	5.89 (1.98)	2.60 (0.83)	–	3.79 (0.24)	1.70 (0.13)	–
	# est.: 10	6.74 (1.03)	2.60 (0.40)	–	7.20 (0.94)	2.35 (0.29)	–	8.76 (0.89)	2.85 (0.33)	–
	# est.: 20	21.21 (4.61)	4.55 (0.99)	–	33.55 (7.48)	6.15 (0.79)	–	22.33 (2.83)	4.40 (0.51)	–
	# est.: 50	115.79 (34.35)	7.80 (1.65)	–	110.24 (32.43)	6.47 (1.39)	3 ($\bar{\rho} = 0.007$)	137.26 (33.37)	8.20 (1.20)	–
	# est.: 100	214.38 (65.07)	6.44 (1.31)	2 ($\bar{\rho} = 0.009$)	274.09 (71.93)	8.87 (1.49)	5 ($\bar{\rho} = 0.004$)	285.62 (95.57)	8.27 (2.02)	9 ($\bar{\rho} = 0.004$)
GBM**	# est.: 5	2.70 (0.22)	1.20 (0.14)	–	2.76 (0.22)	1.85 (0.17)	–	2.37 (0.15)	1.60 (0.13)	–
	# est.: 10	3.20 (0.30)	1.45 (0.15)	–	2.72 (0.29)	2.15 (0.28)	–	4.35 (0.44)	2.75 (0.30)	–
	# est.: 20	5.94 (0.50)	2.60 (0.23)	–	4.25 (0.45)	2.15 (0.28)	–	9.01 (1.11)	3.85 (0.50)	–
	# est.: 50	18.38 (1.62)	4.05 (0.35)	–	24.60 (8.21)	5.85 (1.41)	–	81.33 (28.39)	8.90 (1.36)	–
	# est.: 100	87.11 (26.24)	7.28 (0.77)	2 ($\bar{\rho} = 0.006$)	164.32 (42.12)	11.63 (2.09)	1 ($\bar{\rho} = 0.004$)	137.98 (22.74)	10.33 (0.97)	2 ($\bar{\rho} = 0.007$)
NN	(10,)	1.63 (0.04)	1.00 (0.00)	–	1.55 (0.06)	1.00 (0.00)	–	2.22 (0.19)	1.80 (0.21)	–
	(10, 10, 10)	2.98 (0.15)	1.15 (0.08)	–	2.40 (0.12)	1.15 (0.08)	–	13.01 (3.57)	2.30 (0.40)	–
	(50,)	2.60 (0.14)	1.00 (0.00)	–	2.09 (0.12)	1.05 (0.05)	–	5.75 (0.75)	1.20 (0.12)	–
	(100,)	3.53 (0.15)	1.00 (0.00)	–	4.36 (0.62)	1.10 (0.07)	–	61.31 (33.11)	1.50 (0.22)	10 ($\bar{\rho} = 0.000$)
					$\rho = 0.05$					
Linear	ElasticNet	0.13 (0.00)	–	–	0.15 (0.01)	–	–	0.14 (0.00)	–	–
DT	max depth: 3	1.00 (0.06)	1.70 (0.15)	–	1.09 (0.07)	1.60 (0.15)	–	1.02 (0.07)	1.30 (0.15)	–
	max depth: 5	1.18 (0.11)	1.80 (0.22)	–	1.63 (0.13)	2.05 (0.22)	–	1.33 (0.10)	1.60 (0.18)	–
	max depth: 10	2.22 (0.41)	2.95 (0.61)	–	8.84 (1.49)	4.45 (0.59)	–	3.68 (2.14)	2.95 (1.49)	–
RF*	# est.: 5	2.85 (0.47)	3.25 (0.54)	–	4.29 (0.73)	5.25 (0.86)	–	2.27 (0.19)	2.35 (0.23)	–
	# est.: 10	13.51 (3.03)	8.95 (1.60)	–	14.71 (3.53)	8.35 (1.24)	–	7.41 (1.22)	5.15 (0.67)	–
	# est.: 20	13.86 (3.58)	5.53 (0.92)	1 ($\bar{\rho} = 0.041$)	89.00 (28.17)	14.00 (2.28)	2 ($\bar{\rho} = 0.045$)	47.44 (26.35)	9.50 (2.52)	–
	# est.: 50	101.21 (24.90)	11.37 (1.53)	1 ($\bar{\rho} = 0.048$)	303.27 (93.95)	16.73 (2.55)	9 ($\bar{\rho} = 0.034$)	307.72 (72.52)	19.31 (3.15)	7 ($\bar{\rho} = 0.044$)
	# est.: 100	156.28 (33.21)	8.70 (1.02)	–	453.67 (111.27)	15.43 (2.19)	13 ($\bar{\rho} = 0.032$)	156.45 (116.11)	5.75 (2.29)	16 ($\bar{\rho} = 0.029$)
GBM**	# est.: 5	1.57 (0.15)	1.75 (0.24)	–	1.50 (0.10)	2.05 (0.20)	–	1.97 (0.32)	2.65 (0.50)	–
	# est.: 10	4.84 (0.58)	3.55 (0.46)	–	8.87 (4.44)	8.55 (3.21)	–	11.76 (6.51)	8.85 (3.27)	–
	# est.: 20	12.72 (2.22)	8.28 (0.85)	2 ($\bar{\rho} = 0.038$)	41.81 (17.86)	17.05 (4.37)	1 ($\bar{\rho} = 0.025$)	19.20 (6.32)	9.45 (1.80)	–
	# est.: 50	73.23 (27.00)	13.76 (1.82)	3 ($\bar{\rho} = 0.039$)	223.87 (125.98)	19.86 (4.23)	13 ($\bar{\rho} = 0.027$)	139.18 (56.80)	16.31 (3.03)	7 ($\bar{\rho} = 0.023$)
	# est.: 100	274.22 (51.40)	17.25 (1.57)	4 ($\bar{\rho} = 0.040$)	–	–	20 ($\bar{\rho} = 0.022$)	537.13 (295.04)	15.00 (2.08)	17 ($\bar{\rho} = 0.022$)
NN	(10,)	0.90 (0.01)	1.00 (0.00)	–	1.00 (0.04)	1.15 (0.08)	–	2.96 (0.23)	3.00 (0.25)	–
	(10, 10, 10)	1.48 (0.03)	1.00 (0.00)	–	2.02 (0.26)	1.65 (0.21)	–	229.69 (104.80)	4.90 (0.67)	10 ($\bar{\rho} = 0.039$)
	(50,)	1.39 (0.06)	1.00 (0.00)	–	1.75 (0.13)	1.35 (0.11)	–	19.06 (6.63)	2.37 (0.24)	1 ($\bar{\rho} = 0.049$)
	(100,)	1.83 (0.05)	1.00 (0.00)	–	5.88 (1.19)	1.80 (0.16)	–	289.62 (125.61)	2.70 (0.30)	10 ($\bar{\rho} = 0.000$)

* max depth of each decision tree equal to 3.; ** max depth of each decision tree equal to 2.

Table 1   Generation of robust CEs for 20 factual instances, using ℓ_∞-norm as uncertainty set.

In the first part of the experiments, we analyze our method using three well-known datasets: BANKNOTE AUTHENTICATION, DIABETES, and IONOSPHERE (Dua and Graff

---

[3]https://github.com/donato-maragno/robust-CE

Model	Specs	BANKNOTE AUTHENTICATION 4 features			DIABETES 8 features			IONOSPHERE 34 features		
		Comp. time (s)	# iterations	# early stops	Comp. time (s)	# iterations	# early stops	Comp. time (s)	# iterations	# early stops
					$\rho = 0.01$					
Linear	ElasticNet	0.24 (0.01)	–	–	0.24 (0.01)	–	–	0.26 (0.01)	–	–
DT	max depth: 3	2.09 (0.11)	1.45 (0.11)	–	2.18 (0.13)	1.70 (0.15)	–	5.54 (0.38)	1.20 (0.09)	–
	max depth: 5	2.64 (0.14)	1.53 (0.12)	1 ($\bar{\rho} = 0.000$)	4.21 (0.39)	2.00 (0.23)	–	10.17 (0.78)	1.56 (0.16)	4 ($\bar{\rho} = 0.000$)
	max depth: 10	4.61 (0.88)	2.70 (0.58)	–	14.17 (2.64)	2.63 (0.50)	1 ($\bar{\rho} = 0.000$)	21.75 (2.58)	2.06 (0.26)	2 ($\bar{\rho} = 0.000$)
RF*	# est.: 5	5.20 (0.62)	2.35 (0.34)	–	7.96 (1.65)	3.17 (0.55)	2 ($\bar{\rho} = 0.004$)	69.94 (10.77)	4.41 (0.54)	3 ($\bar{\rho} = 0.006$)
	# est.: 10	10.83 (2.68)	3.41 (0.78)	3 ($\bar{\rho} = 0.006$)	15.20 (3.17)	4.20 (0.68)	–	237.03 (41.12)	5.50 (0.70)	4 ($\bar{\rho} = 0.003$)
	# est.: 20	22.59 (7.10)	4.15 (1.22)	7 ($\bar{\rho} = 0.004$)	104.42 (27.35)	9.81 (1.78)	4 ($\bar{\rho} = 0.007$)	370.21 (41.84)	7.33 (0.73)	5 ($\bar{\rho} = 0.004$)
	# est.: 50	61.93 (14.29)	3.89 (1.22)	11 ($\bar{\rho} = 0.004$)	137.37 (39.96)	6.50 (1.51)	10 ($\bar{\rho} = 0.004$)	570.88 (111.94)	9.70 (1.61)	10 ($\bar{\rho} = 0.001$)
	# est.: 100	103.33 (31.75)	3.20 (0.89)	10 ($\bar{\rho} = 0.004$)	177.47 (41.01)	3.80 (0.86)	15 ($\bar{\rho} = 0.002$)	531.13 (121.00)	6.17 (0.98)	14 ($\bar{\rho} = 0.001$)
GBM**	# est.: 5	4.50 (0.50)	2.50 (0.34)	–	4.67 (0.47)	2.45 (0.26)	–	11.47 (1.48)	4.42 (0.66)	8 ($\bar{\rho} = 0.002$)
	# est.: 10	6.87 (0.88)	3.15 (0.42)	–	6.11 (1.04)	2.70 (0.48)	–	42.68 (6.67)	6.88 (0.86)	3 ($\bar{\rho} = 0.001$)
	# est.: 20	14.02 (1.09)	4.40 (0.34)	–	10.97 (1.45)	3.65 (0.49)	–	58.16 (7.01)	9.62 (1.00)	4 ($\bar{\rho} = 0.004$)
	# est.: 50	34.03 (3.15)	5.21 (0.44)	1 ($\bar{\rho} = 0.010$)	76.04 (33.09)	9.35 (2.21)	–	192.70 (42.52)	14.77 (2.47)	7 ($\bar{\rho} = 0.006$)
	# est.: 100	133.53 (24.40)	8.50 (0.98)	6 ($\bar{\rho} = 0.007$)	201.13 (77.68)	12.08 (2.92)	8 ($\bar{\rho} = 0.005$)	415.96 (80.09)	17.29 (3.36)	13 ($\bar{\rho} = 0.003$)
NN	(10,)	1.64 (0.09)	1.00 (0.00)	–	1.73 (0.05)	1.00 (0.00)	–	4.73 (0.57)	1.27 (0.19)	9 ($\bar{\rho} = 0.004$)
	(10, 10, 10)	2.54 (0.15)	1.00 (0.00)	–	2.04 (0.10)	1.00 (0.00)	6 ($\bar{\rho} = 0.000$)	282.24 (193.65)	1.50 (0.50)	18 ($\bar{\rho} = 0.003$)
	(50,)	2.42 (0.14)	1.00 (0.00)	–	2.00 (0.08)	1.00 (0.00)	1 ($\bar{\rho} = 0.000$)	48.13 (12.76)	2.40 (0.51)	15 ($\bar{\rho} = 0.008$)
	(100,)	3.57 (0.14)	1.00 (0.00)	–	5.28 (0.83)	1.15 (0.11)	–	352.64 (153.96)	1.09 (0.09)	9 ($\bar{\rho} = 0.000$)
					$\rho = 0.05$					
Linear	ElasticNet	0.15 (0.00)	–	–	0.34 (0.02)	–	–	0.26 (0.01)	–	–
DT	max depth: 3	1.72 (0.17)	2.25 (0.19)	–	6.71 (0.65)	2.40 (0.24)	–	4.40 (1.35)	2.60 (0.90)	–
	max depth: 5	2.69 (0.52)	3.95 (0.74)	1 ($\bar{\rho} = 0.026$)	20.28 (2.88)	5.00 (0.68)	1 ($\bar{\rho} = 0.000$)	5.91 (1.09)	2.26 (0.40)	1 ($\bar{\rho} = 0.000$)
	max depth: 10	4.44 (0.80)	4.95 (0.93)	–	178.35 (34.48)	9.11 (1.30)	1 ($\bar{\rho} = 0.045$)	20.91 (10.20)	5.05 (1.51)	–
RF*	# est.: 5	4.49 (0.64)	4.40 (0.64)	–	117.95 (28.96)	9.63 (1.82)	1 ($\bar{\rho} = 0.049$)	28.79 (2.76)	6.35 (0.51)	–
	# est.: 10	12.39 (2.57)	6.82 (1.14)	3 ($\bar{\rho} = 0.048$)	200.39 (69.46)	12.92 (2.93)	7 ($\bar{\rho} = 0.043$)	232.63 (36.46)	10.79 (1.36)	1 ($\bar{\rho} = 0.042$)
	# est.: 20	51.29 (18.03)	10.17 (2.32)	8 ($\bar{\rho} = 0.049$)	149.39 (46.57)	12.75 (2.78)	12 ($\bar{\rho} = 0.042$)	450.46 (68.06)	8.50 (1.06)	10 ($\bar{\rho} = 0.027$)
	# est.: 50	93.18 (51.21)	7.78 (2.17)	11 ($\bar{\rho} = 0.048$)	560.78 (–)	6.00 (–)	19 ($\bar{\rho} = 0.031$)	510.69 (341.34)	7.50 (3.50)	18 ($\bar{\rho} = 0.021$)
	# est.: 100	108.47 (29.76)	5.25 (0.80)	8 ($\bar{\rho} = 0.047$)	868.10 (–)	4.00 (–)	19 ($\bar{\rho} = 0.024$)	495.03 (268.88)	9.00 (2.08)	17 ($\bar{\rho} = 0.014$)
GBM**	# est.: 5	2.67 (0.33)	3.55 (0.47)	–	8.89 (1.29)	3.68 (0.53)	1 ($\bar{\rho} = 0.000$)	11.38 (1.83)	5.74 (0.68)	1 ($\bar{\rho} = 0.029$)
	# est.: 10	5.77 (0.45)	5.55 (0.44)	–	46.46 (14.33)	12.00 (3.12)	–	72.15 (15.31)	15.19 (2.62)	4 ($\bar{\rho} = 0.005$)
	# est.: 20	23.89 (3.55)	10.41 (1.00)	3 ($\bar{\rho} = 0.046$)	153.43 (43.11)	18.76 (3.73)	3 ($\bar{\rho} = 0.036$)	156.17 (19.16)	16.42 (1.71)	8 ($\bar{\rho} = 0.005$)
	# est.: 50	123.75 (51.10)	18.14 (4.47)	6 ($\bar{\rho} = 0.044$)	243.24 (80.72)	24.50 (6.31)	14 ($\bar{\rho} = 0.029$)	894.23 (100.35)	32.50 (6.50)	18 ($\bar{\rho} = 0.013$)
	# est.: 100	389.06 (124.83)	20.25 (3.32)	12 ($\bar{\rho} = 0.044$)	– (–)	– (–)	20 ($\bar{\rho} = 0.020$)	– (–)	– (–)	20 ($\bar{\rho} = 0.010$)
NN	(10,)	0.91 (0.00)	1.00 (0.00)	–	4.13 (0.13)	1.00 (0.00)	–	36.34 (5.22)	1.68 (0.19)	1 ($\bar{\rho} = 0.000$)
	(10, 10, 10)	1.45 (0.03)	1.00 (0.00)	–	8.02 (0.86)	1.31 (0.18)	4 ($\bar{\rho} = 0.024$)	328.70 (72.59)	2.38 (0.35)	4 ($\bar{\rho} = 0.012$)
	(50,)	1.36 (0.03)	1.00 (0.00)	–	11.27 (1.10)	1.50 (0.15)	–	57.07 (7.28)	1.22 (0.10)	2 ($\bar{\rho} = 0.000$)
	(100,)	2.26 (0.04)	1.00 (0.00)	–	26.82 (3.39)	1.30 (0.13)	–	111.85 (26.18)	1.44 (0.24)	11 ($\bar{\rho} = 0.001$)

* max depth of each decision tree equal to 3.; ** max depth of each decision tree equal to 2.

Table 2   **Generation of robust CEs for 20 factual instances, using ℓ_2-norm as uncertainty set.**

2017). Before training the ML models, we scaled each feature to be between zero and one. None of the datasets contain categorical features, which otherwise would have been considered immutable or fixed according to the user's preference. We apply our algorithm to generate robust CEs for 20 factual instances randomly selected from the dataset. We use ℓ_∞-norm as uncertainty set with a radius (ρ) of 0.01 and 0.05. For each instance, we use a time limit of 1000 seconds. Although less practical from a user's perspective, we also report the results using ℓ_2-norm as uncertainty set in Table 2. The datasets used in our analysis do not require any additional constraints, such as *actionability*, *sparsity*, or *data manifold closeness*. However, it is important to note that these types of constraints can be added to our formulations when needed by using constraints like the ones proposed in (Maragno et al. 2022). The accuracy of each trained ML model is provided in Appendix C.

In Table 1, we show (from left to right) the type of ML model, model-specific hyperparameters, and for each dataset, the average computation time (in seconds), the number of iterations performed by the algorithm, and the number of instances where the algorithm

hits the time limit without providing an optimal solution. For the computation time and the number of iterations, we show the standard error values in parentheses. For the early stops, we show the (average) maximum radius of the uncertainty set, which is feasible for the generated counterfactual solutions in each iteration of the algorithm. The latter value gives a measure for the robustness of the returned solution. As for hyperparameters, we report the maximum tree depth for DT, the number of generated trees for RF and GBM, and the depth of each layer in the NN. The results indicate that the computation time and the number of iterations increase primarily due to the complexity of the ML models rather than the number of features in the datasets. This complexity can also be a consequence of model overfitting. In Figure 6, we illustrate this by visualizing the iterations for a DT with a maximum depth of (a) 10 and (b) 3. As can be observed, the more complex model substantially increases the number of iterations, and hence the computation time.
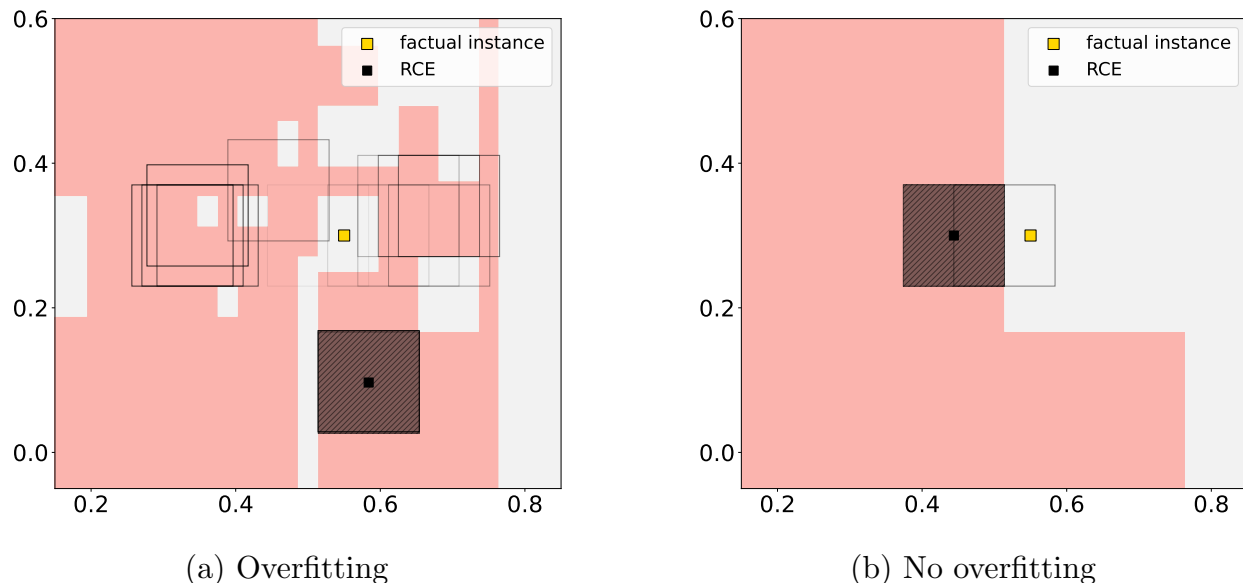

(a) Overfitting (b) No overfitting

Figure 6   **Comparison of decision trees with different maximum depths. The decision tree on the right has a maximum depth of 3, while the one on the right has a maximum depth of 10 and is overfitted. The overfitted decision tree leads to a higher number of iterations needed to find a robust solution, as shown by the larger number of boxes/solutions generated before converging.**

When the time limit is reached, we can still provide a list of solutions generated by solving the (MP) at each iteration. Each one of these solutions comes with information on the distance to the actual instance and the radius of the uncertainty set for which the model predictions still belong to the desired class for all perturbations. Therefore, the

decision-makers still have the chance to select CEs from a region, albeit slightly smaller than intended. Overall the algorithm converges relatively quickly, however, our experiments show that it converges slower when using ℓ_2-norm as uncertainty set; see Table 2. Furthermore, as expected, for a smaller radius of $\rho = 0.01$ we reach the global optimum faster. Figure 7 shows the convergence behavior of various predictive models trained on the DIABETES dataset and evaluated on a specific instance. Although the distance to the factual instance (solid line) follows a monotonic increasing trend, the robustness (dashed line) exhibits both peaks and troughs. This behavior can be attributed to the objective function of (MP), which seeks to minimize the distance between the CE and the factual instance. With each iteration of our algorithm, a new scenario/constraint is introduced to (MP), resulting in a worse objective value (higher), but not necessarily an improvement in robustness.
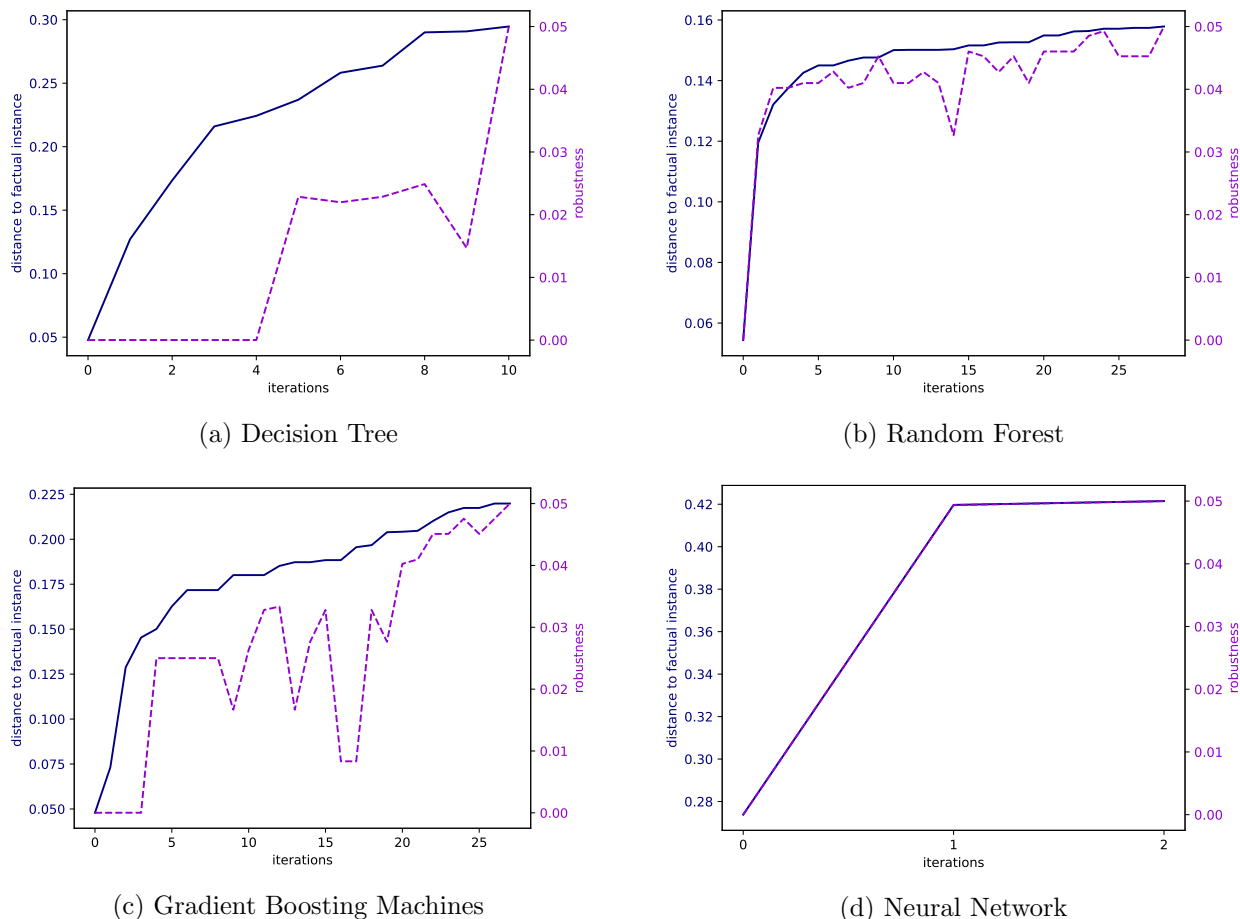

(a) Decision Tree

(b) Random Forest

(c) Gradient Boosting Machines

(d) Neural Network

Figure 7   Convergence plots for DT with max depth 10 (a), RF with 50 trees (b), GBM with 50 trees (c), and NN with one hidden layer containing 100 nodes (d). The models are trained on the Diabetes dataset and the uncertainty set is the ℓ_∞-norm.

ρ	Dominguez-Olmedo et al. (2021)		Our algorithm	
	robustness	validity	robustness	validity
	BANKNOTE NN(50)			
0.1	80%	100%	100%	100%
0.2	0%	100%	100%	100%
	DIABETES NN(50)			
0.1	60%	100%	100%	100%
0.2	0%	100%	80%	100%
	IONOSPHERE NN(10)			
0.1	70%	90%	100%	100%
0.2	40%	90%	100%	100%
	IONOSPHERE NN(50)			
0.1	50%	100%	100%	100%
0.2	30%	100%	100%	100%

Table 3   Comparison between (Dominguez-Olmedo et al. 2021) and our algorithm regarding the percentage of times each algorithm was able to find a counterfactual at least ρ distant from the decision boundary, and the percentage of times the counterfactual explanations were valid and therefore resulting in a flip in the prediction.

In the latter part of the experiment, we train a neural network with one hidden layer containing 50 nodes using the same three datasets. For the IONOSPHERE dataset, we also trained another neural network with one hidden layer containing 10 nodes. To generate robust counterfactuals, we used the ℓ_2-norm uncertainty set and tested our algorithm against the one proposed by Dominguez-Olmedo et al. (2021) on 10 instances. In Table 3, we report the percentage of times each algorithm was able to find a counterfactual that was at least ρ distant from the decision boundary (robustness) and the percentage of times the counterfactual was valid (validity). We test ρ values of 0.1 and 0.2 for each dataset. Our approach consistently generated counterfactual explanations that were optimal in terms of distance to the factual instance and valid. However, in the DIABETES dataset, our algorithm failed to find a robust counterfactual in 20% of the cases. In contrast, the algorithm proposed by Dominguez-Olmedo et al. (2021) often returned solutions that were not entirely robust with respect to ρ, particularly with the increase in ρ and the complexity of the predictive model. Even more concerning, their algorithm generated invalid solutions in 10% of the cases for the IONOSPHERE dataset. Note that our experiments only cover neural network models since the method in (Dominguez-Olmedo et al. 2021) cannot be used for non-differentiable predictive models.

5. Discussion and Future Work

In this paper, we propose a robust optimization approach for generating regions of CEs for tree-based models and neural networks. We have also shown theoretically that our approach converges. This result has also been supported by empirical studies on different datasets. Our experiments demonstrate that our approach is able to generate explanations efficiently on a variety of datasets and ML models. Our results indicate that the proposed method scales well with the number of features and that the main computational challenge lies in solving the master problem as it becomes larger with every iteration. Overall, our results suggest that our proposed approach is a promising method for generating robust CEs for a variety of machine learning models.

As future work, we plan to investigate methods for speeding up the calculations of the master problem by using more efficient formulations of the predictive models. Additionally, we aim to evaluate the user perception of the robust CEs generated by our approach and investigate how the choice of the uncertainty set affects the quality of the solution. Another research direction is the implementation of categorical and immutable features into the model, which would require a reformulation of the uncertainty set to account for the different feature types. This would lead to non-convex, discrete, and lower-dimensional uncertainty sets.

Acknowledgments

Appendix A: Linear Models

Although Algorithm 1 could still be used for the linear models, there is a well-known easier, and more efficient dual approach to solve model (3)-(4). We review this approach briefly here for the completeness of our discussion.

In the case of linear models, such as logistic regression (LR) or linear support vector machines (SVM), the validity constraint (4) can be formulated as

$$\boldsymbol{\beta}^\top (\boldsymbol{x} + \boldsymbol{s}) + \beta_0 \geq \tau, \quad \forall \boldsymbol{s} \in \mathcal{S}, \tag{68}$$

where $\boldsymbol{\beta} \in \mathbb{R}^n$ is the coefficient vector and $\beta_0 \in \mathbb{R}$ is the intercept. Then, these constraints can be equivalently reformulated as

$$\boldsymbol{\beta}^\top \boldsymbol{x} + \beta_0 + \min_{\boldsymbol{s} \in \mathcal{S}} \beta^\top \boldsymbol{s} \geq \tau.$$

Since $\mathcal{S}$ is given in the form (5), the latter is equivalent to

$$\boldsymbol{\beta}^\top \boldsymbol{x} - \rho ||\boldsymbol{\beta}||^* + \beta_0 \geq \tau, \tag{69}$$

where $\| \cdot \|^*$ is the dual norm of the norm used in the definition of $\mathcal{S}$. The constant term $\rho ||\boldsymbol{\beta}||^*$ ensures that the constraint (68) holds for all $\boldsymbol{s} \in \mathcal{S}$. Note that constraint (69) remains linear in $\boldsymbol{x}$ independently of $\mathcal{S}$. For more details see, *e.g.*, Dominguez-Olmedo et al. (2021), Bertsimas et al. (2019), Xu et al. (2008).

Appendix B: Proof of Lipschitz Continuity of Neural Networks

Suppose that we have a trained ℓ-layer neural network constructed with ReLU activation functions. If we denote the resulting functional by $f : \mathbb{R}^{n_0} \mapsto \mathbb{R}^{n_\ell}$, then we can write

$$f(\boldsymbol{x}) = \sigma_\ell(W_\ell \sigma_{\ell-1}(W_{\ell-1}\sigma_{\ell-2} \ldots W_2 \sigma_1(W_1 \boldsymbol{x}) \ldots)), \tag{70}$$

where $\sigma_m : \mathbb{R}^{n_m} \mapsto \mathbb{R}^{n_m}$, $m = 1, \ldots, \ell$ stands for the vectorized ReLU functions, and $W_m \in \mathbb{R}^{n_m} \times \mathbb{R}^{n_{m-1}}$, for $m = 1, \ldots, \ell$, are the weight matrices. This shows that f is simply the composition of linear and component- as well as piece-wise linear functions.

Given any two Lipschitz continuous functions $g : \mathbb{R}^p \mapsto \mathbb{R}^q$ and $h : \mathbb{R}^q \mapsto \mathbb{R}^s$ with respective Lipschitz constants L_g and L_h, the composition $h \circ g : \mathbb{R}^p \mapsto \mathbb{R}^p$ is Lipschitz continuous with Lipschitz constant $L_h L_g$. This simply follows from observing for a pair of vectors $\boldsymbol{y}, \boldsymbol{z} \in \mathbb{R}^p$ that

$$\|h \circ g(\boldsymbol{y}) - h \circ g(\boldsymbol{z})\| \leq L_h \|g(\boldsymbol{y}) - g(\boldsymbol{z})\| \leq L_h L_g \|\boldsymbol{y} - \boldsymbol{z}\|. \tag{71}$$

Next, for any $\boldsymbol{u}, \boldsymbol{v} \in \mathbb{R}^{n_m}$, we have

$$\|W_m \boldsymbol{u} - W_m \boldsymbol{v}\| \leq \|W_m\|_s \|\boldsymbol{u} - \boldsymbol{v}\|. \tag{72}$$

where $\| \cdot \|_s$ is the spectral norm. As the Lipschitz constant for any vectorized ReLU function is one, we obtain the desired result by

$$\|f(\bar{\boldsymbol{x}}) - f(\tilde{\boldsymbol{x}})\| \leq \prod_{m=1}^{\ell} \|W_m\|_s \|\bar{\boldsymbol{x}} - \tilde{\boldsymbol{x}}\| \tag{73}$$

for any pair $\bar{\boldsymbol{x}}, \tilde{\boldsymbol{x}} \in \mathbb{R}^{n_0}$. $\qquad \square$

Appendix C: Performances of Predictive Models

	LR	CART			RF					GBM					NN			
		3	**5**	**10**	**5**	**10**	**20**	**50**	**100**	**5**	**10**	**20**	**50**	**100**	**(10)**	**(10, 10, 10)**	**(50)**	**(100)**
									BANKNOTE									
Train	0.97	0.94	0.98	1.00	0.96	0.97	0.96	0.97	0.97	0.99	0.99	1.00	1.00	1.00	0.98	0.99	1.00	1.00
Test	0.96	0.89	1.00	1.00	0.96	0.93	0.93	0.96	0.93	0.96	1.00	1.00	1.00	1.00	1.00	1.00	1.00	1.00
									DIABETES									
Train	0.77	0.77	0.84	0.97	0.77	0.77	0.79	0.80	0.80	0.80	0.83	0.87	0.93	0.99	0.78	0.79	0.80	0.82
Test	0.72	0.77	0.72	0.69	0.72	0.69	0.69	0.67	0.71	0.59	0.67	0.69	0.59	0.62	0.69	0.64	0.73	0.77
									IONOSPHERE									
Train	0.88	0.93	0.97	1.00	0.93	0.95	0.94	0.96	0.96	0.99	1.00	1.00	1.00	1.00	0.98	0.99	0.99	0.99
Test	0.83	0.88	0.83	0.83	0.88	0.92	0.92	0.92	0.92	0.88	0.88	0.92	0.92	0.92	0.89	0.92	0.88	0.88

Table 4   **Train and test accuracy scores of the predictive models used for the experiments.**

Table 4 displays the accuracy score of each predictive model employed in the experiments, with their performance being reported for both the training and testing sets.

References

Anderson R, Huchette J, Ma W, Tjandraatmadja C, Vielma JP (2020) Strong mixed-integer programming formulations for trained neural networks. *Mathematical Programming* 183(1-2):3–39, ISSN 14364646, URL http://dx.doi.org/10.1007/s10107-020-01474-5.

Artelt A, Vaquet V, Velioglu R, Hinder F, Brinkrolf J, Schilling M, Hammer B (2021) Evaluating robustness of counterfactual explanations. *2021 IEEE Symposium Series on Computational Intelligence (SSCI)* 01–09, URL http://dx.doi.org/10.1109/ssci50451.2021.9660058.

Ben-Tal A, El Ghaoui L, Nemirovski A (2009) *Robust Optimization* (Princeton University Press), ISBN 9781400831050, URL http://dx.doi.org/10.1515/9781400831050.

Bertsimas D, Dunn J, Pawlowski C, Zhuo YD (2019) Robust classification. *INFORMS Journal on Optimization* 1(1):2–34.

Black E, Wang Z, Fredrikson M, Datta A (2021) Consistent counterfactuals for deep models. URL http://dx.doi.org/10.48550/ARXIV.2110.03109.

Bui N, Nguyen D, Nguyen VA (2022) Counterfactual plans under distributional ambiguity.

Cplex II (2009) V12. 1: User's manual for CPLEX. *International Business Machines Corporation* 46(53):157.

Dandl S, Molnar C, Binder M, Bischl B (2020) Multi-objective counterfactual explanations. Bäck T, Preuss M, Deutz A, Wang H, Doerr C, Emmerich M, Trautmann H, eds., *Parallel Problem Solving from Nature – PPSN XVI*, 448–469 (Cham: Springer International Publishing), ISBN 978-3-030-58112-1.

Dominguez-Olmedo R, Karimi AH, Schölkopf B (2021) On the adversarial robustness of causal algorithmic recourse. URL http://dx.doi.org/10.48550/ARXIV.2112.11313.

Dua D, Graff C (2017) UCI machine learning repository. URL http://archive.ics.uci.edu.

Dutta S, Long J, Mishra S, Tilli C, Magazzeni D (2022) Robust counterfactual explanations for tree-based ensembles. Chaudhuri K, Jegelka S, Song L, Szepesvari C, Niu G, Sabato S, eds., *Proceedings of the 39th International Conference on Machine Learning*, volume 162 of *Proceedings of Machine Learning Research*, 5742–5756 (PMLR), URL https://proceedings.mlr.press/v162/dutta22a.html.

Ferrario A, Loi M (2022) The robustness of counterfactual explanations over time. *IEEE Access* 10:82736–82750, URL http://dx.doi.org/10.1109/ACCESS.2022.3196917.

Forel A, Parmentier A, Vidal T (2022) Robust counterfactual explanations for random forests. URL http://dx.doi.org/10.48550/ARXIV.2205.14116.

Grimstad B, Andersson H (2019) ReLU networks as surrogate models in mixed-integer linear programs. *Computers and Chemical Engineering* 131:106580, ISSN 00981354, URL http://dx.doi.org/10.1016/j.compchemeng.2019.106580.

Gurobi Optimization, LLC (2022) Gurobi optimizer reference manual. URL https://www.gurobi.com.

Kanamori K, Takagi T, Kobayashi K, Ike Y, Uemura K, Arimura H (2021) Ordered counterfactual explanation by mixed-integer linear optimization. *Proceedings of the AAAI Conference on Artificial Intelligence* 35(13):11564–11574.

Karimi AH, Barthe G, Balle B, Valera I (2020) Model-agnostic counterfactual explanations for consequential decisions. Chiappa S, Calandra R, eds., *Proceedings of the Twenty Third International Conference on Artificial Intelligence and Statistics*, volume 108 of *Proceedings of Machine Learning Research*, 895–905 (PMLR).

Mahajan D, Tan C, Sharma A (2019) Preserving causal constraints in counterfactual explanations for machine learning classifiers. URL `http://dx.doi.org/10.48550/ARXIV.1912.03277`.

Maragno D, Röber TE, Birbil I (2022) Counterfactual explanations using optimization with constraint learning. URL `http://dx.doi.org/10.48550/ARXIV.2209.10997`.

Maragno D, Wiberg H, Bertsimas D, Birbil SI, den Hertog D, Fajemisin A (2021) Mixed-integer optimization with constraint learning. URL `http://dx.doi.org/10.48550/ARXIV.2111.04469`.

Mothilal RK, Sharma A, Tan C (2020) Explaining machine learning classifiers through diverse counterfactual explanations. *Proceedings of the 2020 Conference on Fairness, Accountability, and Transparency* 607–617.

Mutapcic A, Boyd S (2009) Cutting-set methods for robust convex optimization with pessimizing oracles. *Optimization Methods & Software* 24(3):381–406.

Pawelczyk M, Datta T, van-den Heuvel J, Kasneci G, Lakkaraju H (2022) Probabilistically robust recourse: Navigating the trade-offs between costs and robustness in algorithmic recourse. URL `http://dx.doi.org/10.48550/ARXIV.2203.06768`.

Rawal K, Kamar E, Lakkaraju H (2020) Algorithmic recourse in the wild: Understanding the impact of data and model shifts. URL `http://dx.doi.org/10.48550/ARXIV.2012.11788`.

Russell C (2019) Efficient search for diverse coherent explanations. *Proceedings of the Conference on Fairness, Accountability, and Transparency* 20–28.

Slack D, Hilgard A, Lakkaraju H, Singh S (2021) Counterfactual explanations can be manipulated. Ranzato M, Beygelzimer A, Dauphin Y, Liang P, Vaughan JW, eds., *Advances in Neural Information Processing Systems*, volume 34, 62–75 (Curran Associates, Inc.).

Upadhyay S, Joshi S, Lakkaraju H (2021) Towards robust and reliable algorithmic recourse. Ranzato M, Beygelzimer A, Dauphin Y, Liang P, Vaughan JW, eds., *Advances in Neural Information Processing Systems*, volume 34, 16926–16937 (Curran Associates, Inc.).

Ustun B, Spangher A, Liu Y (2019) Actionable recourse in linear classification. *Proceedings of the Conference on Fairness, Accountability, and Transparency* 10–19.

Virgolin M, Fracaros S (2023) On the robustness of sparse counterfactual explanations to adverse perturbations. *Artificial Intelligence* 316:103840, ISSN 0004-3702, URL `http://dx.doi.org/https://doi.org/10.1016/j.artint.2022.103840`.

Wachter S, Mittelstadt B, Russell C (2018) Counterfactual explanations without opening the black box: automated decisions and the GDPR. *Harvard Journal of Law and Technology* 31(2):841–887.

Xu H, Caramanis C, Mannor S (2008) Robust regression and lasso. *Advances in Neural Information Processing Systems* 21.